Fabrication of anodic porous alumina via anodizing in cyclic oxocarbon acids

Tatsuya Kikuchi, Daiki Nakajima, Jun Kawashima, Shungo Natsui, and Ryosuke O. Suzuki
Faculty of Engineering, Hokkaido University
N13-W8, Kita-ku, Sapporo, Hokkaido, 060-8628, Japan

*Corresponding author: Tatsuya Kikuchi
TEL: +81-11-706-6340
FAX: +81-11-706-6342
E-mail: kiku@eng.hokudai.ac.jp

Abstract

The growth behavior of anodic porous alumina formed by anodizing in novel electrolyte solutions, the cyclic oxocarbon acids croconic and rhodizonic acid, was investigated for the first time. High-purity aluminum specimens were anodized in 0.1 M croconic and rhodizonic acid solutions at various constant current densities. An anodic porous alumina film with a cell size of 200-450 nm grew uniformly on an aluminum substrate by rhodizonic acid anodizing at 5-40 Am^{-2}, and a black, burned oxide was formed at higher current density. The cell size of the porous alumina increased with current density and corresponding anodizing voltage. Anodizing in croconic acid at 293 K caused the formation of thin anodic porous alumina films as well as black, thick burned oxides. The uniformity of the porous alumina improved by increasing the temperature of the croconic acid solution, and anodic porous alumina films with a uniform film thickness were successfully obtained. Our experimental results showed that the cyclic oxocarbon acids croconic and rhodizonic acid could be employed as a suitable electrolyte for the formation of anodic porous alumina films.

Key words: Aluminum; Anodizing; Anodic Porous Alumina; Croconic Acid; Rhodizonic Acid

1. Introduction

The anodizing of aluminum in several different acidic solutions causes the formation of anodic porous alumina (i.e., porous anodic oxide film) with characteristic nanofeatures on aluminum substrates. Porous alumina consists of nano-scale hexagonal cells perpendicular to the substrate, and each cell possesses a nanopore at its center [1,2]. These cells are self-ordered by anodizing under appropriate electrochemical conditions, especially under a high electric field [3,4]. When anodic porous alumina is immersed in boiling distilled water after anodizing, the nanopores are filled by hydroxide (pore-sealing) [5,6]. The sealing process causes the formation of a highly crystalline hydroxide layer on the surface of the anodic oxide, and the hydroxide layer is highly dissolution-resistant in acidic and alkaline solutions. Using these characteristic structural and chemical properties, anodic porous alumina has been widely investigated for many applications: antireflection structures [7,8], reflectors [9], memory devices [10], diodes [11], sensors [12], optical devices [13,14], nanocontainers [15], plasmonic devices [16], nano-templates [17,18], evaporation masks [19], catalyst supports [20], resist masks [21,22], and corrosion protection [23,24].

The electrolytes used to fabricate anodic porous alumina can be clearly classified by the use of the following two chemical species: inorganic and organic acids. Four types of electrolytes based on the following inorganic acids have been reported to date for the fabrication of anodic porous alumina: sulfuric (H_2SO_4) [25-27], phosphoric (H_3PO_4) [28-30], chromic (H_2CrO_4) [31-33], and selenic (H_2SeO_4) [34] acid. Among these inorganic electrolytes, the use of sulfuric, phosphoric, and selenic acid for anodizing under suitable anodizing conditions results in the formation of highly ordered anodic porous alumina via self-ordering. On the other hand, poorly arranged nanoporous structures are formed by chromic acid anodizing due to pore branching. Several carboxylic acids, including oxalic ($(COOH)_2$) [35-38], malonic (HOOC-CH_2-COOH) [39-41], tartalic (HOOC-$(CHOH)_2$-COOH) [42-44], citric (HOOC-CH_2-C(OH)(COOH)-CH_2-COOH) [45-47], malic (HOOC-CH(OH)-CH_2-COOH) [45,48], glycolic (HOOC-CH_2OH) [45], formic (HCOOH) [49], and tartronic (HOOC-CH(OH)-COOH) [50] acid have been reported to date for the fabrication of anodic porous alumina. Oxalic and malonic acid anodizing have been reported to give rise to self-ordering behavior under suitable anodizing conditions. The organic and inorganic electrolytes used to fabricate anodic porous alumina possess low dissociation constant (pKa) in aqueous solution, except for glycolic and formic acid, are diacids or triacids. However, glycolic and formic acid form dimers via hydrogen bonding in aqueous solution and may behave like diacids [52,53]. The nanofeatures of anodic porous alumina, including cell size (i.e., interpore distance) and pore diameter, are limited by these electrolytes during anodizing. Therefore, the discovery of additional electrolytes is very important in expanding the applicability of porous alumina. However, it is a well-known experimental fact that anodic porous alumina cannot be formed by anodizing in many organic and inorganic acid solutions

[48]. Indeed, to date, there have been no reports of available organic electrolytes, except for carboxylic acid, that can be used to this end. This limitation may thus presents an obstacle to further expanding to the nanomorphologies of anodic porous alumina.

Very recently, we discovered a new organic electrolyte for anodic porous alumina fabrication, squaric acid (3,4-dihydroxy-3-cyclobutene-1,2-dione) [54], which is different from the carboxylic acids described above. Squaric acid is currently the most popular cyclic oxocarbon acid used in organic chemistry and is a strong diacid composed of two acidic hydroxyl groups with low dissociation constants of $pKa_1 = 0.5$ and $pKa_2 = 3.5$ [55]. Squaric acid anodizing is performed at voltages of 100-150 V under typical anodizing conditions [54]. An anodic porous alumina film with micrometer-scale thickness, submicron-scale-cell size, and sub-100-nm-scale pore diameter can be successfully obtained by squaric acid anodizing. These findings demonstrate that anodic porous alumina can also be fabricated by anodizing in organic acids other than carboxylic acids.

Oxocarbon acids such as squaric acid are widely investigated in the field of organic synthetic chemistry. Figure 1 summarizes characteristics of the members of the series of cyclic oxocarbon acids that have been reported to date. Deltic acid, with a three-membered ring, was first synthesized by Eggerding et al. in 1975 [56]. Although deltic acid possesses low diacid dissociation constants ($pKa_1 = 2.6$ and $pKa_2 = 6.0$) [57], similarly to squaric acid, the acid is difficult to use as an anodizing electrolyte because it easily decomposes in aqueous and ethanol solutions [56]. Croconic acid, with a five-membered ring, and rhodizonic acid, with a six-membered ring, are long-known chemical species whose detailed chemical structures were only recently determined. Croconic acid possesses low pKa values of 0.8 and 2.2 [57,58], and similarly, rhodizonic acid possesses low pKa values of 4.3 and 4.7 [57,59,60]. Heptagonic acid, with a seven-membered ring, is not commercially available at the present time, although the possibility of synthesizing heptagonic acid was reported by Seits et al. [61] Based on the considerations outlined above, it is strongly believed that croconic and rhodizonic acid have the potential to behave as suitable electrolytes for the fabrication of anodic porous alumina.

In the present report, we describe the fabrication of an anodic porous alumina films with uniform thickness via croconic and rhodizonic acid anodizing. Anodic porous alumina was successfully fabricated by constant current anodizing in croconic and rhodizonic acid solutions under suitable electrochemical conditions. The growth behavior of the porous alumina films and their nanomorphologies were examined in detail by electrochemical measurements and electron microscope observations.

2. Experimental

High-purity aluminum foils (99.99 wt%, 110 μm thick, 20 mm × 20 mm with a handle, Showa Aluminum Co., Japan) were used as the starting materials. In the present investigation, no electropolishing was carried out to avoid the delay of anodic porous

alumina formation, as reported previously [43,48]. The aluminum specimens were ultrasonically degreased in C_2H_5OH for 10 min, and a silicone resin was then coated on the bottom of the handle. After drying the coated silicone resin, the specimens were immersed in 0.1 M croconic acid (T = 293-323 K, pH = 1.17 at room temperature, 4,5-Dihydroxy-4-cyclopentene-1,2,3-trione, Tokyo Chemical Industry, Japan) and 0.1 M rhodizonic acid (T = 293 K, pH = 1.72 at room temperature, 5,6-Dihydroxy-5-cyclohexene-1,2,3,4-tetrone, Santa Cruz Biotechnology, USA) solutions and then anodized for up to 60 min at constant current densities of i = 5-80 Am^{-2}. The electrochemical anodizing setup consisted of a simple two-electrode system, in which a platinum plate was used as the counter electrode. The croconic and rhodizonic acid solutions were stirred with a magnetic stirrer during anodizing, and the temperature was maintained at a constant value using a water bath. The corresponding anodizing voltage during constant current anodizing was recorded by a PC-controlled direct current power supply (PWR-400H, Kikusui, Japan). After anodizing, the specimens were immediately removed from solution and then washed with distilled water and dried in a desiccator.

The anodized specimens were immersed in a 0.20 M CrO_3/0.51 M H_3PO_4 solution (T = 353 K) for up to 30 min to selectively dissolve the anodic oxide. Through this treatment, the interface between the anodic oxide and the aluminum substrate, which corresponds to the growth plane of the anodic oxide, was exposed to the surface. The nanomorphologies of the surface and the interface of the anodized specimens were examined by field-emission scanning electron microscopy (FE-SEM, JIB-4600F/HKD, JEOL). The crystallinity of the anodic oxide was determined by X-ray diffraction (XRD, XpertPro, Phillips). A vertical cross-section of the anodic oxide was observed after preparing two treated specimens: a) the anodized specimens were embedded in an epoxy resin (EpoFix, Struers) and polished mechanically, and b) the specimens were mechanically cut. For the observation of the anodic oxide, a thin platinum conductive layer was coated on the oxide by a sputter coater (MSP-1S, Vacuum Device, Japan).

3. Results and discussion

3.1 Growth behavior of the anodic porous alumina formed by rhodizonic acid anodizing

Figure 2 shows the changes in anodizing voltage, V, with anodizing time, t_a, in a 0.1 M rhodizonic acid solution at 293 K and constant current densities of i_a = 5, 10, 20, 40, and 80 Am^{-2} over a period of 60 min. At i_a = 5 Am^{-2}, the anodizing voltage showed an increase of 2-3 V during the initial stage of anodizing. This voltage increase corresponds a thin, native oxide film on the aluminum substrate. The voltage then increased linearly with anodizing time due to the formation of a barrier anodic oxide film via the following electrochemical reaction [1]:

$$2Al + 3H_2O = Al_2O_3 + 6H^+ + 6e^- \quad (1)$$

With the linear increase in the voltage, the thickness of the barrier layer increased with anodizing time; in other words, the thickness increased with anodizing voltage. After

this increase, the voltage reached a maximum value of V = 87 V at t_a = 22 min and then slightly decreased with anodizing time. Lastly, the voltage remained at a steady value of 78 V for the remainder of the anodizing period. This current-time behavior, characterized by the appearance of a maximum value, a slight decrease, and the appearance of a steady value, is typically measured by anodizing in other acidic solutions such as sulfuric, oxalic, and phosphoric acid for anodic porous alumina fabrication [1]. The slight decrease observed corresponds to the formation of nanopores in the barrier oxide, and the plateau region corresponds to the steady-state growth of the anodic porous alumina. During the growth of the anodic porous alumina film, the voltage maintained a steady value due to a balance between oxide dissolution at the pore bottom and oxide formation at the interface between the oxide and the aluminum substrate. Therefore, the voltage-time curve at i_a = 5 Am^{-2} strongly suggests that anodic porous alumina was formed on the aluminum substrate by rhodizonic acid anodizing.

At i_a = 5-80 Am^{-2} (Fig. 2), the slope of the linear increase in voltage for the barrier oxide film became much steeper as the current density increased. This behavior was due to the increase in the growth rate of the barrier oxide under high-current-density anodizing. Accordingly, the anodizing voltage for porous alumina also increased with current density. In addition, the voltages at i_a = 20 and 40 Am^{-2} during the steady-state growth of the porous alumina slightly increased with anodizing time. At i = 80 Am^{-2}, the voltage oscillated between 160 and 200 V during anodizing after the linear voltage increase, and there was a sudden drop at t_a = 40 min. This electrochemical behavior is clearly different from that observed at other current densities. Figure 2 shows that rhodizonic acid anodizing occurs over a wide range of anodizing voltages of approximately 80-200 V.

Figure 3 shows the surface appearance of the specimens anodized in rhodizonic acid solution for 60 min; the changes in the anodizing voltages measured for these specimens are shown in Fig. 2. The as-received aluminum foil showed a metallic luster with white and light-gray coloring. After anodizing at i_a = 5-10 Am^{-2}, the specimens showed the formation of a thin oxide layer with uniform light-purple and green coloring due to interference. As the current density increased (20 and 40 Am^{-2}), the color of the anodic oxide gradually became a slightly reddish, dark gray due to the increase in the thickness of the anodic oxide. At i_a = 80 Am^{-2}, a black oxide region was observed on the upper left of the anodized specimen, although the dark-gray anodic oxide was also formed in the other regions. The formation of such as black film is typically induced by the very high current density resulting from the high electric field applied during anodizing, a phenomenon called “burning” [43,62]. In the burning phenomenon, the local thickening of the anodic oxide occurs and corresponding black oxides are produced. The formation of this non-uniform oxide by burning may have caused the unstable, oscillatory voltage behavior observed during anodizing (Fig. 2). For the specimens fabricated by stable anodizing in rhodizonic acid solution at i_a = 5-40 Am^{-2}, the nanomorphology of the anodic oxides was examined by FE-SEM.

Figure 4a) shows an SEM image of the fracture cross-section of the specimen anodized in rhodizonic acid solution at i_a = 40 Am^{-2} for 60 min; the specimen was prepared by being mechanically cut. An anodic oxide film measuring 3.4 μm in thickness was uniformly formed on the aluminum substrate, and numerous nanopores formed from the top surface to the bottom interface in the anodic oxide. A typical amorphous pattern of the anodic oxide was detected by XRD measurements of the anodized specimen. A high-magnification SEM image of the top surface of the anodized specimen is shown in Fig. 4b (the observed area is surrounded by a yellow square in Fig. 4a). Nanopores measuring approximately a few 10 nm to 100 nm in diameter were generated from the surface of the anodic oxide in a disorderly fashion, and the diameter of the nanopores in the inner anodic oxide became larger than that of the nanopores on the surface because of the rearrangement of the porous layer during long periods of anodizing [63]. Figure 4c) shows a high-magnification SEM image of the bottom interface of the anodic oxide indicated by a light-green square in Fig. 4a). Barrier oxides featuring a thin hemispherical oxide film were clearly observed at the bottom of the anodic layer. An anodic porous alumina film was also successfully obtained by rhodizonic acid anodizing at other current densities, as demonstrated in Fig. 2. From the electrochemical measurements and SEM observations reported in Fig. 2 through Fig. 4, rhodizonic acid can be clearly identified as a new anodizing electrolyte for anodic porous alumina fabrication.

Figure 5a) shows an SEM image of the vertical cross-section of the specimen anodized at i_a = 40 Am^{-2} for 60 min. The anodized specimen was embedded in an epoxy resin. In the figure, the black region at the top corresponds to the epoxy resin and the gray region with a rough surface at the bottom corresponds to the aluminum substrate. An anodic porous alumina film with a uniform thickness measuring approximately 7 μm was formed on the aluminum substrate, and numerous, straight nanopores were observed in the anodic oxide. Based on observations of a large area of the cross-sectional specimen, the uniform porous alumina film was formed over the entire surface of the aluminum substrate, and no crack or any other imperfection was observed in the anodic porous alumina film. Changes in the thickness of the anodic porous alumina, δ, with current density, i_a, except in the case of burning (i_a = 80 Am^{-2}), are shown in Fig. 5b). It is clearly observed that the thickness of the porous alumina increased linearly with current density under the uniform growth conditions. This proportional relationship between the thickness and current density suggests that steady-state anodic oxidation, in the absence of any other anodic reaction such as oxygen gas evolution, occurred on the aluminum specimen during rhodizonic acid anodizing at these constant current densities.

When the anodized specimen was immersed in CrO_3/H_3PO_4 solution at high temperature, the anodic oxide was selectively dissolved into the solution, and the aluminum substrate was exposed to the surrounding environment. The exposed aluminum showed nanodimple periodic structures corresponding to the bottom shape of

the anodic porous alumina. Thus, the growth behavior of the anodic porous alumina film fabricated by rhodizonic acid anodizing could be monitored by observing the exposed aluminum surface. Figure 6a) shows SEM images of the exposed aluminum surface after rhodizonic acid anodizing at i_a = 5-40 Am^{-2} for 60 min; the anodic oxides were completely dissolved by selective dissolution. At i_a = 5 Am^{-2}, disordered nanodimples measuring approximately 200 nm in diameter were distributed on the aluminum substrate. As the current density increased during anodizing, the mean diameter of the nanodimples increased with the current density, and the regularity of the nanodimple array was also improved. The diameter of the nanodimples corresponds to the cell size (or interpore distance) of the anodic porous alumina. In general, there is linear relation between the anodizing voltage and the cell size formed by anodizing, and the relation is described as follows [45]:

$$D = 2.5\ V \quad (2)$$

where D is the cell size. Figure 6b) shows the change in the cell size, D, with the anodizing voltage, V, measured by anodizing for 60 min at different current densities. The cell size is directly proportional to the anodizing voltage with a proportional constant of 2.5 nmV^{-1}, and this relation is in fair agreement with that reported previously, which was obtained by anodizing in other electrolytes such as sulfuric, oxalic, and phosphoric acid solutions.

In summary, anodic porous alumina films with a uniform thickness can be successfully fabricated by anodizing in rhodizonic acid solution. Rhodizonic acid anodizing occurs over a wide anodizing voltage range of approximately 80-180 V, and anodic porous alumina with a corresponding cell size of 200-450 nm can be formed on an aluminum substrate. It is expected that such uniform and robust anodic porous alumina films can be used to direct the nanostructure fabrication and surface finishing of aluminum substrates, although further investigation of rhodizonic acid anodizing under various electrochemical conditions is required.

3.2 Growth behavior of the anodic porous alumina formed by croconic acid anodizing

Rhodizonic acid anodizing successfully allowed for the fabrication of uniform anodic porous alumina films. In this section, the growth behavior of anodic oxide in croconic acid solution is discussed. Figure 7 shows the changes in anodizing voltage, V, with anodizing time, t_a, at different current densities, i_a = 5-80 Am^{-2} during anodizing in a 0.1 M croconic acid solution at 293 K. Typical voltage-time transients, including voltage jumps, a linear increase during the initial stage of anodizing, the appearance of a peak value, and a subsequent slight decrease, for anodic porous alumina formation were measured by croconic acid anodizing at different current densities. Unlike in rhodizonic acid anodizing, the voltages measured after the appearance of a peak value at each current density showed a relatively high voltage range of 150-175 V, and these voltages slightly decreased with anodizing time, except for the voltage measured at i_a = 10 Am^{-2}. In addition, no smooth voltage-time curves were obtained at i_a = 10 and 20 A m^{-2}. In the

case of such unstable anodizing behavior, it is expected that non-uniform anodic oxide may have been formed on the aluminum substrate.

Figure 8 shows the surface appearance of the specimens anodized in croconic acid solution for 60 min at different current densities. At i_a = 5 Am^{-2}, an anodic oxide with light-gray coloring was formed on the aluminum specimen. The surface appearance of the specimen anodized at i_a = 10 Am^{-2} was similar to that anodized i_a = 5 Am^{-2}, but it was observed that black, burned oxides were formed at the top and edges of the aluminum specimen. These burned oxides were clearly formed on the surface of the specimen anodized at i_a = 20 Am^{-2} and became larger with increasing current density (i_a = 40 Am^{-2}). Lastly, half of the specimen surface was covered by burned oxides at i_a = 80 A m^{-2}. The unstable electrochemical behavior demonstrated in Fig. 7 may be due to this burned oxide formation during anodizing. In fact, such characteristic burned oxides were not formed by rhodizonic acid anodizing under low-current-density conditions (i_a = 5-40 A m^{-2}). These light-gray anodic oxides and black, burned oxides formed by croconic acid anodizing were examined in detail by SEM as follows.

Figure 9a) shows an SEM image of the surface of the specimens anodized in croconic acid solution for 60 min at i_a = 20 Am^{-2}. A typical, uniform light-gray region, as shown in Fig. 8, was observed. The striped pattern observed from the top to the bottom of the figure corresponds to the marks formed by the rolling process during aluminum foil manufacturing. Numerous nanopores measuring approximately 50 nm in diameter were formed over the entire region demarcated by the light-gray anodic oxide. A fracture cross-section of the anodic oxide, which was prepared by mechanical cutting, is shown in Fig. 9b). An anodic oxide film measuring less than 1 μm in thickness was formed on the aluminum substrate, and characteristic vertical nanopores and a barrier oxide at the bottom of the oxide were clearly observed. Based on these SEM observations, croconic acid can also be identified as a new anodizing electrolyte for anodic porous alumina fabrication. However, the anodic porous alumina film formed by croconic acid anodizing at i_a = 20 Am^{-2} was much thinner than that formed by rhodizonic acid anodizing (3.4 μm, Fig. 5b), although the same current density was applied in both anodizing procedures. This discrepancy was due to the local thickening of burned oxide during croconic acid anodizing, as indicated in Fig. 10 and will be discussed later. Figure 9c) shows a magnified image of the nanodimple array formed on the anodic porous alumina film shown in Figs. 9a) and 9b). Disordered nanodimples were distributed throughout the aluminum substrate, and many defects formed at the fourth and fifth points of the nanodimple junctions due to incomplete self-ordering.

A cross-sectional SEM image of the black, burned oxide formed by croconic acid anodizing at i_a = 80 Am^{-2} is shown in Fig. 10a). Several lens-shaped burned oxides, measuring approximately 200 μm in wide and 100 μm in thickness, were observed. Thin porous oxides measuring approximately 1 μm in thickness were also formed in the region between the burned oxides (i.e., except for the burned region). This local thickening of the anodic oxide is typically observed when anodizing under the burning

conditions [43,62], and similar structures have also been observed during the selective growth of anodic porous alumina films in micro-sized areas of aluminum substrates exposed by imperfections and laser irradiation [65-67]. In addition, it was observed that the burned oxides possessed several cracks measuring a few micrometers in width from the surface and throughout their thickness. These cracks resulted in stress generated by the volume expansion of the anodic oxide. In fact, the Pilling-Bedworth ratio (P-B ratio) for aluminum and its oxide is approximately 1.5 [68], and thus, the oxide should expand after anodizing.

Figure 10b) shows an SEM image of the nanodimple array formed under the burned oxide layer. Unlike in Fig. 9c), it is clear that nanodimples measuring approximately 250 nm were ordered on the aluminum substrate, although several imperfections still remained. This well-defined, highly ordered nanodimple array resulted in a high growth rate under high-current-density anodizing in localized regions due to the burning of the anodic porous alumina layer. In fact, it has been previously reported that the self-ordering of porous alumina can be generally achieved under high electric fields induced at high current densities [69]. This ordered array formed by croconic acid anodizing suggests that self-ordering over the entire surface is achieved by "hard anodizing" (i.e., constant-voltage anodizing under a high electric field) with a powerful cooling setup, as previously reported [69].

Figures 7 through 10 demonstrate that croconic acid anodizing causes the non-uniform formation of an anodic porous alumina layer, although a porous alumina film can successfully be formed on the aluminum. To form a uniform anodic porous alumina film by constant-current anodizing and also to prevent the local thickening of the anodic oxide, we observed that constant-current anodizing at high temperature was required. Figure 11 shows the changes in anodizing voltage, V, with anodizing time, t_a, during croconic acid anodizing at i_a = 40 Am^{-2} and different solution temperatures ranging from 293 to 323 K. At 293 K, the anodizing voltage slightly decreased with anodizing time after the initial transients associated with the onset of nanopore formation. In contrast, as the temperature of the croconic acid solution was increased to 308 and 323 K, the voltage increased with the anodizing time over the initial transient regions. These current-time transients are very similar to those obtained by rhodizonic acid anodizing at i_a = 40 Am^{-2}. Thus, it is expected that the growth behavior of the anodic porous alumina is altered under high-temperature croconic acid anodizing. Based on the images of the specimen surfaces (insert images in Fig. 11)), uniform anodic oxides without black, burned oxides were formed on the anodized specimens.

Figure 12a) shows an SEM image of the vertical cross-section of a specimen anodized in croconic acid solution at 323 K and then mechanically polished. It is clearly observed that an anodic porous alumina film measuring 5.2 μm in thickness was uniformly formed on the aluminum substrate. No burned oxide or any other imperfection was observed over the entire region of the anodic oxide by SEM. The anodic oxide formed by croconic acid anodizing consisted of only an amorphous layer,

as indicated by XRD. By anodizing at high temperature, the uniform growth of the anodic oxide at the oxide/aluminum interface and the uniform dissolution of the oxide at the pore bottom may be accelerated (Fig. 10a)). Therefore, croconic acid anodizing at high temperature allowed for the formation of a uniform and smooth anodic porous oxide without burning. The thickness of the anodic oxide formed by croconic acid anodizing (δ = 5.2 μm) was smaller than that formed by rhodizonic acid anodizing (δ = 6.9 μm, Fig. 5b)), although the two types of films were anodized at the same current density of i_a = 40 Am^{-2}, due to the active dissolution of aluminum into solution during croconic acid anodizing at high temperature [63]. The SEM images of a fracture cross-section shown in Figs. 12b) and c) indicate that nanopores measuring approximately 100 nm in diameter were formed in the porous layer. In addition, several instances of pore-branching and dead pores were observed in the porous alumina layer due to disordered growth.

In summary, non-uniform anodic oxides, including black, burned oxides and thin porous oxides, were formed on aluminum by croconic acid anodizing at low temperature. Although regions of disordered anodic porous alumina were distributed over the thin oxide, highly ordered porous regions were formed at the burned oxides due to the high electric field applied during anodizing under burning conditions. The uniformity of the anodic oxide was greatly improved by anodizing at high temperature, and an anodic porous alumina film with a uniform thickness could be successfully fabricated. Therefore, croconic acid anodizing is also useful for surface finishing and nanostructuring applications. Based on the experimental results obtained in our previous study [54] and those obtained in this work, the cyclic oxocarbon acids, squaric, croconic, and rhodizonic acid, form suitable electrolytes for anodic porous alumina fabrication. Thus, heptagonic acid (Fig. 1) may also be suitable for anodic porous alumina fabrication, although it is currently difficult to chemically synthesize the acid. Comparing croconic acid anodizing with rhodizonic acid anodizing at 293 K, the different growth behaviors were observed: anodic porous alumina films with a uniform thickness could be obtained in rhodizonic acid solution, but thin porous alumina with several black, burned oxides was formed in croconic acid solution. Typically, anodizing in organic acid solutions (i. e., dicarboxylic acids) with high pKa and pH values tends to easily cause burning of the anodic oxide. However, the pKa and pH values of croconic acid solution are lower than that of rhodizonic acid solution, and there is no agreement on that point. Therefore, effect of electrolyte characteristic on anodizing behavior should be further investigated to understand the mechanism of aluminum anodizing.

4. Conclusions

We described the fabrication of anodic porous alumina films formed by anodizing in novel electrolytes, croconic and rhodizonic acid under constant-current-density conditions. The following conclusions may be drawn from the results of the electrochemical measurements and SEM observations.

1) Anodic porous alumina can be fabricated via constant-current anodizing in 0.1 M croconic and rhodizonic acid solutions.
2) Rhodizonic acid anodizing at a constant current density of i_a = 5-40 Am^{-2} and 293 K allows for the formation of uniform anodic porous alumina films, whereas regions of burned oxide are formed at a higher current density of i_a = 80 Am^{-2}. The cell size of the porous alumina film increases with the current density and corresponding anodizing voltage.
3) Non-uniform burned oxide regions and thin anodic porous alumina layers are formed by croconic acid anodizing at 293 K. The locally formed burned oxide regions form a highly ordered nanostructure. High-temperature croconic acid anodizing allows for the formation of anodic porous alumina films of uniform thickness.

Acknowledgments

This research was conducted at Hokkaido University and was supported by the "Nanotechnology Platform" Program of the Ministry of Education, Culture, Sports, Science, and Technology (MEXT), Japan. This work was financially supported by the Japan Society for the Promotion of Science (JSPS) "KAKENHI" and Toyota Physical & Chemical Research Institute Scholars.

References

1) G.E. Thompson, Porous anodic alumina: fabrication, characterization and applications, Thin Solid Films 297 (1997) 192-201.
2) Ö.Ö. Çapraz, P. Shrotriya, K.R. Hebert, Measurement of Stress Changes during Growth and Dissolution of Anodic Oxide Films on Aluminum, J. Electrochem. Soc. 161 (2014) D256-D262.
3) H. Masuda, K. Fukuda, Ordered metal nanohole arrays made by a two-step replication of honeycomb structures of anodic alumina, Science 268 (1995) 1466-1468.
4) S. Ono, M. Saito, M. Ishiguro, H. Asoh, Controlling factor of self-ordering of anodic porous alumina, J. Electrochem. Soc. 151 (2004) B473-B478.
5) M. Koda, H. Takahashi, M. Nagayama, Reaction of porous anodic oxide films on aluminum with hot water I. Effect of film thickness and reaction time on the degree of hydration and acid-dissolution characteristics, J. Surf. Fin. Soc. Jpn. 33 (1982) 242-248 (1982).
6) H. Jha, T. Kikuchi, M. Sakairi, H. Takahashi, Area-selective microscale metallization on porous anodic oxide film of aluminium, Electrochem. Commun. 9 (2007) 1596-1601.
7) T. Yanagishita, M. Masui, N. Ikegawa, H. Masuda, Fabrication of polymer antireflection structures by injection molding using ordered anodic porous alumina mold, J. Vac. Sci. Technol. B 32 (2014) 021809.
8) T. Yanagishita, K. Nishio, H. Masuda, Anti-reflection structures on lenses by nanoimprinting using ordered anodic porous alumina, Appl. Phys. Express 2, (2009) 022001.
9) G.D. Sulka, K. Hnida, Distributed Bragg reflector based on porous anodic alumina fabricated by pulse anodization, Nanotechnology 23, (2012) 075303.
10) D. Liu, C. Zhang, G. Wang, Z. Shao, X. Zhu, N. Wang, H. Cheng, Nanoscale electrochemical metallization memories based on amorphous (La, Sr) MnO_3 using ultrathin porous alumina masks, J. Phys. D: Appl. Phys. 47 (2014) 085108.
11) S. Zhang, L. Wang, C. Xu, D. Li, L. Chen, D. Yang, Fabrication of Ni-NiO-Cu Metal-Insulator-Metal Tunnel Diodes via Anodic Aluminum Oxide Templates, ECS Solid State Lett. 2 (2013) Q1-Q4.
12) E. Kurowska, A. Brzózka, M. Jarosz, G.D. Sulka, M. Jaskuła, Silver nanowire array sensor for sensitive and rapid detection of H_2O_2, Electrochim. Acta 104, (2013) 439-447.
13) Q. Lin, B. Hua, S. Leung, X. Duan, Z. Fan, Efficient light absorption with integrated nanopillar/nanowell arrays for three-dimensional thin-film photovoltaic applications, ACS Nano 7 (2013) 2725-2732.
14) T. Yanagishita, K. Nishio, H. Masuda, Fabrication of two-dimensional polymer photonic crystals by nanoimprinting using anodic porous alumina mold, J. Vac. Sci. Technol. B 28 (2010) 398-400.

15) X. Zhao, G. Meng, F. Han, X. Li, B. Chen, Q. Xu, X. Zhu, Z. Chu, M. Kong, Q. Huang, Nanocontainers made of various materials with tunable shape and size, Sci. Rep. 3 (2013) 2238.
16) S. Shukla, K.T. Kim, A. Baev, Y.K. Yoon, N.M. Litchinitser, P.N. Prasad, Fabrication and Characterization of Gold− Polymer Nanocomposite Plasmonic Nanoarrays in a Porous Alumina Template, ACS Nano 4 (2010) 2249-2255.
17) A.B. Papandrew, R.W. Atkinson III, G.A. Goenaga, S.S. Kocha, J.W. Zack, B.S. Pivovar, T.A. Zawodzinski Jr., Oxygen Reduction Activity of Vapor-Grown Platinum Nanotubes, J. Electrochem. Soc. 160 (2013) F848-F852.
18) M. Santamaria, L. Asaro, P. Bocchetta, B. Megna, F.Di. Quarto, Electrodeposition of CeO_2 and Co-Doped CeO_2 Nanotubes by Cyclic Anodization in Porous Alumina Membranes, ECS Electrochem. Lett. 2 (2013) D29-D32.
19) H. Masuda, K. Yasui, K. Nishio, Fabrication of ordered arrays of multiple nanodots using anodic porous alumina as an evaporation mask, Adv. Mater. 12 (2000) 1031-1033.
20) J.C. Ganley, K.L. Riechmann, E.G. Seebauer, R.I. Masel, Porous anodic alumina optimized as a catalyst support for microreactors, J. Catal. 227 (2004) 26-32.
21) T. Kikuchi, Y. Wachi, T. Takahashi, M. Sakairi, R.O. Suzuki, Fabrication of a meniscus microlens array made of anodic alumina by laser irradiation and electrochemical techniques, Electrochim. Acta 94 (2013) 269-276.
22) T. Kikuchi, Y. Wachi, M. Sakairi, R.O. Suzuki, Aluminum bulk micromachining through an anodic oxide mask by electrochemical etching in an acetic acid/perchloric acid solution, Microelectron. Eng. 111 (2013) 14-20.
23) V.R. Capelossi, M. Poelman, I. Recloux, R.P.B. Hermandes, H.G. de Melo, M.G. Olivier, Corrosion protection of clad 2024 aluminum alloy anodized in tartaric-sulfuric acid bath and protected with hybrid sol–gel coating, Electrochim. Acta 124 (2014) 6979.
24) T. Kikuchi, Y. Hara, M. Sakairi, T. Yonezawa, A. Yamauchi, H. Takahashi, Corrosion of Al–Sn–Bi alloys in alcohols at high temperatures. Part II: Effect of anodizing on corrosion, Corr. Sci. 52 (2010) 2525-2534.
25) H. Masuda, F. Hasegawa, S. Ono, Self-Ordering of Cell Arrangement of Anodic Porous Alumina Formed in Sulfuric Acid Solution, J. Electrochem. Soc. 144 (1997) L127-L130.
26) G.D. Sulka, S. Stroobants, V. Moshchalkov, G. Borghs, J.-P. Celis, Synthesis of well-ordered nanopores by anodizing aluminum foils in sulfuric acid, J. Electrochem. Soc. 149 (2002) D97-D103.
27) J. Martín, C.V. Manzano, O. Caballero-Calero, M. Martín-González, High-aspect-ratio and highly ordered 15-nm porous alumina templates, ACS Appl. Mater. Interfaces 5 (2013) 72-79.
28) H. Masuda, K. Yada, A. Osaka, Self-ordering of cell configuration of anodic porous alumina with large-size pores in phosphoric acid solution, Jpn. J. Appl. Phys. 37

(1998) L1340.
29) A.P. Li, F. Müller, A. Birner, K. Nielsch, U. Gösele, Hexagonal pore arrays with a 50–420 nm interpore distance formed by self-organization in anodic alumina, J. Appl. Phys. 84 (1998) 6023-6026.
30) I. Vrublevsky, V. Parkoun, J. Schreckenbach, Analysis of porous oxide film growth on aluminum in phosphoric acid using re-anodizing technique, Appl. Surf. Sci. 242 (2005) 333-338.
31) S.J. Garcia-Vergara, P. Skeldon, G.E. Thompson, H. Habazaki, A tracer investigation of chromic acid anodizing of aluminium, Surf. Interface Anal. 39 (2007) 860-864.
32) W.J. Stępniowski, M. Norek, M. Michalska-Domańska, A. Bombalska, A. Nowak-Stępniowska, M. Kwaśny, Z. Bojar, Fabrication of anodic aluminum oxide with incorporated chromate ions, Appl. Surf. Sci. 259 (2012) 324-330.
33) W.J. Stępniowski, M. Michalska-Domańska, M. Norek, T. Czujko, Fast Fourier transform based arrangement analysis of poorly organized alumina nanopores formed via self-organized anodization in chromic acid, Mater. Lett. 117 (2014) 69-73.
34) O. Nishinaga, T. Kikuchi, S. Natsui, R.O. Suzuki, Rapid fabrication of self-ordered porous alumina with 10-/sub-10-nm-scale nanostructures by selenic acid anodizing, Sci. Rep. 3 (2013) 2748.
35) G.D. Sulka, W. J. Stępniowski, Structural features of self-organized nanopore arrays formed by anodization of aluminum in oxalic acid at relatively high temperatures, Electrochim. Acta 54 (2009) 3683-3691.
36) G.D. Sulka, A. Brzózka, L. Zaraska, M. Jaskuła, Through-hole membranes of nanoporous alumina formed by anodizing in oxalic acid and their applications in fabrication of nanowire arrays, Electrochim. Acta 55 (2010) 4368-4376.
37) W.J. Stępniowski, A. Nowak-Stępniowska, M. Michalska-Domańska, M. Norek, T. Czujko, Z. Bojar, Fabrication and geometric characterization of highly-ordered hexagonally arranged arrays of nanoporous anodic alumina, Pol. J. Chem. Tech. 16 (2014) 63-69.
38) W.J. Stępniowski, M. Norek, M. Michalska-Domańska, D. Forbot, A. Król, Study on the correlation between criterion number derived from Rayleigh–Bénard convective cells and arrangement of nanoporous anodic aluminum oxide, Mater. Lett. 125 (2014) 124-127.
39) W. Lee, K. Nielsch, U. Gösele, Self-ordering behavior of nanoporous anodic aluminum oxide (AAO) in malonic acid anodization, Nanotechnology 18 (2007) 475713.
40) I. Vrublevsky, A. Jagminas, S. Hemeltjen, W. Goedel, Behavior of acid species during heat treatment and re-anodizing of porous alumina films formed in malonic acid, J. Solid. State. Electrochem. 13 (2009) 1873-1880.
41) B. Sun, J. Li, X. Jin, C. Zhou, Q. Hao, X. Gao, Self-ordered hard anodization in malonic acid and its application in tailoring alumina taper-nanopores with

continuously tunable periods in the range of 290–490nm, Electrochim. Acta 112 (2013) 327-332.
42) V.F. Surganov, G.G. Gorokh, Anodic oxide cellular structure formation on aluminum films in tartaric acid electrolyte, Mater. Lett. 17 (1993) 121-124.
43) S. Ono, M. Saito, H. Asoh, Self-ordering of anodic porous alumina formed in organic acid electrolytes, Electrochimica Acta 51 (2005) 827-833.
44) I.A. Vrublevsky, K.V. Chernyakova, A. Ispas, A. Bund, S. Zavadski, Optical properties of thin anodic alumina membranes formed in a solution of tartaric acid, Thin Solid Films 556 (2014) 230-235.
45) S.Z. Chu, K. Wada, S. Inoue, M. Isogai, Y. Katsuta, A. Yasumori, Large-scale fabrication of ordered nanoporous alumina films with arbitrary pore intervals by critical-potential anodization, J. Electrochem. Soc. 153 (2006) B384-B391.
46) Y. Katsuta, A. Yasumori, K. Wada, K. Kurashima, S. Suehara, S. Inoue, Three-dimensionally nanostructured alumina film on glass substrate: Anodization of glass surface, J. Non-Cryst. Solids 354 (2008) 451-455.
47) J. Bellemare, F. Sirois, D. Ménard, Fabrication of Micrometer-Scale Self-Organized Pore Arrays in Anodic Alumina, J. Electrochem. Soc. 161 (2014) E75-E80.
48) T. Kikuchi, T. Yamamoto, R.O. Suzuki, Growth behavior of anodic porous alumina formed in malic acid solution, Appl. Surf. Sci. 284 (2013) 907-913.
49) T. Fukushima, Y. Fukuda, G. Ito, Y. Sato, Anodic oxidation of local corrosion of aluminum in mono-carboxylic acids, J. Surf. Fin. Soc. Jpn. 21 (1970) 319-326.
50) M. Pashchanka, J. Schneider, Experimental validation of the novel theory explaining self-organization in porous anodic alumina films, Phys. Chem. Chem. Phys. 15 (2013) 7070-7074.
51) T. Kikuchi, O. Nishinaga, S. Natsui, R.O. Suzuki, Fabrication of Anodic Porous Alumina via Acetylenedicarboxylic Acid Anodizing, ECS Electrochem. Lett. 3 (2014) C25-C28.
52) J. Chocholoušová, V. Špirko, P. Hobza, First local minimum of the formic acid dimer exhibits simultaneously red-shifted O–HO and improper blue-shifted C–HO hydrogen bonds, Phys. Chem. Chem. Phys. 6 (2004) 37-41.
53) N. ElBakali-Kassimi, E.F. Archibong, A.J. Thakkar, Hydrogen bonding in the glycolic acid dimer, J. Mol. Structure 591 (2002) 189-197.
54) T. Kikuchi, T. Yamamoto, S. Natsui, R.O. Suzuki, Fabrication of Anodic Porous Alumina by Squaric Acid Anodizing, Electrochim. Acta 123 (2014) 14-22.
55) K. Aknin, M. Gauriot, J. Totobenazara, N. Deguine, R. Deprez-Poulain, B. Deprez, J. Charton, Squaric acid is a suitable building-block in 4C-Ugi reaction: access to original bivalent compounds, Tetrahedron Lett. 53 (2012) 458-461.
56) D. Eggerding, R. West, Synthesis of dihydroxycyclopropenone (deltic acid), J. Am. Chem. Soc. 97 (1975) 207-208.
57) G.V. Perez, A.L. Perez, Organic acids without a carboxylic acid functional group, J. Chem. Educ. 77 (2000) 910-915.

58) L.M. Schwarts, R.I. Gelb, J.O. Yardley, Aqueous dissociation of croconic acid, J. Phys, Chem. 79 (1975) 2246-2251.
59) E. Patton, R. West, New aromatic anions. VIII. acidity constants of rhodizonic acid, J. Phys, Chem. 74 (1970) 2512-2518.
60) R.I. Gelb, L.M. Schwarts, D.A. Laufer, The structure of aqueous rhodizonic acid, J. Am. Chem. Soc. 82 (1978) 1985-1988.
61) G. Seitz, P. Imming, Oxocarbons and pseudooxocarbons, Chem. Rev. 92 (1992) 1227-1260.
62) T. Aerts, I. De Graeve, H. Terryn, Study of initiation and development of local burning phenomena during anodizing of aluminium under controlled convection, Electrochim. Acta 54 (2008) 270-279.
63) C. Chuan, K.Y. Ng, N.R. Aluru, A.H.W. Ngan, Simulation and experiment of substrate aluminum grain orientation dependent self-ordering in anodic porous alumina, J. Appl. Phys. 113 (2013) 204903.
64) M. Koda, H. Takahashi, S. Nagayama, The effect of current density and temperature on the anodic oxidation of aluminum in sulfuric and oxalic acid solutions, J. Surf. Fin. Soc. Jpn. 28 (1977) 584-588.
65) T.A. Renshaw, A study of pore structures on anodized aluminum, J. Electrochem. Soc. 108 (1961) 185-191.
66) H. Takahashi, M. Nagayama, H. Akahori, A. Kitahara, Electron-microscopy of Porous Anodic Oxide Films on Aluminium by Ultra-thin Sectioning Technique: Part 1. The Structrual Change of the Film during the Current Recovery Period, J. Electron Microsc. 22 (1973) 149-157.
67) T. Kikuchi, M. Sakairi, H. Takahashi, Growth of porous type anodic oxide films at micro-areas on aluminum exposed by laser irradiation, Electrochim. Acta 54 (2009) 7018-7024.
68) A. Mozalev, S. Magaino, H. Imai, The formation of nanoporous membranes from anodically oxidized aluminium and their application to Li rechargeable batteries, Electrochim. Acta 46 (2001) 2825-2834.
69) W. Lee, R. Ji, U. Gösele, K. Nielsch, Fast fabrication of long-range ordered porous alumina membranes by hard anodization, Nature Mater. 5 (2006) 741747.

Captions

Figure 1. Summary of the characteristics of cyclic oxocarbon acids and thier dissociation constants (pKa_1 and pKa_2). Five oxocarbon acids have been reported to date: deltic, squaric, croconic, rhodizonic, and heptagonic acid.

Figure 2. Changes in anodizing voltage, V, with time, t_a, during anodizing in a 0.1 M rhodizonic acid solution for 60 min at constant current densities in the range of i_a = 5-80 A m^{-2}.

Figure. 3 Surface appearance of the specimens anodized in a 0.1 M rhodizonic acid solution for 60 min at different current densities. As-received aluminum foil with a metallic luster was also examined.

Figure 4 a) SEM image of the fracture cross-section of an anodic oxide film formed by rhodizonic acid anodizing at i_a = 40 A m^{-2} for 60 min. The anodized specimen was mechanically cut for observation. b) and c) High-magnification SEM images of the b) top surface and c) bottom interface of an anodic oxide film, indicated by yellow and green squares in a), respectively.

Figure 5 a) Low-magnification SEM image of the vertical cross-section of an anodic oxide formed by rhodizonic acid anodizing at i_a = 40 A m^{-2} for 60 min. The specimen was embedded in an epoxy resin and then mechanically polished. b) Change in thickness of the anodic porous alumina film, δ, with current density, i_a, during rhodizonic acid anodizing.

Figure 6 a) SEM images of the nanodimple array formed on the aluminum substrate by rhodizonic acid anodizing at different current densities. To examine the dimple arrays, the anodized specimens were immersed in a CrO_3/H_3PO_4 solution to selectively dissolve the anodic porous alumina. b) The relationship between the anodizing voltage and the cell size for anodic porous alumina formed in rhodizonic acid solution.

Figure 7 Changes in anodizing voltage, V, with time, t_a, during anodizing in a 0.1 M croconic acid solution for 60 min at constant current densities in the range of i_a = 5-80 A m^{-2}.

Figure 8 Surface appearance of the specimens anodized in a 0.1 M croconic acid solution for 60 min at different current densities.

Figure 9 SEM images of the a) surface, b) fracture cross-section, and c) dimple array of the specimen anodized in a 0.1 M croconic acid solution at 293 K and i_a = 20 Am^{-2}.

Figure 10 a) SEM image of the vertical cross-section of a specimen anodized in croconic acid solution at i_a = 80 Am^{-2}. b) SEM image of the well-ordered nanodimple array formed under the burned oxide shown in a).

Figure 11 Changes in anodizing voltage, V, with time, t_a, during croconic acid anodizing for 60 min at different temperatures between 293 and 323 K and i_a = 40 A m^{-2}.

Figure 12 SEM images of the a) vertical and b) fracture cross-section of the specimens anodized in croconic acid solution at 323 K and i_a = 40 A m^{-2} for 60 min. c) High-magnification SEM image of the bottom of a nanopore.

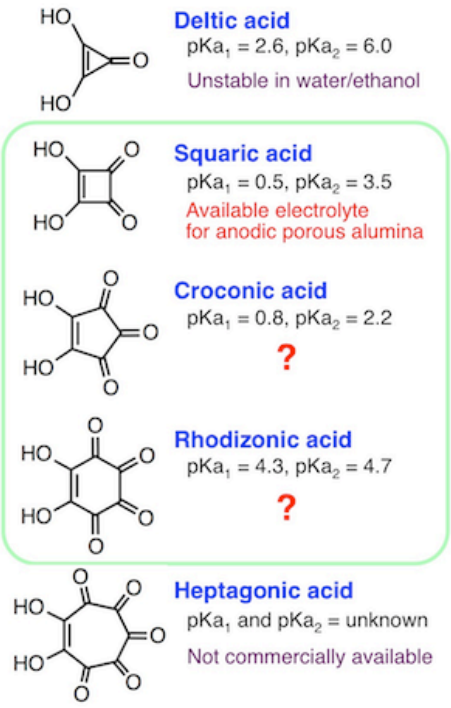
Deltic acid
pKa1 = 2.6, pKa2 = 6.0
Unstable in water/ethanol
Squaric acid
pKa1 = 0.5, pKa2 = 3.5
Available electrolyte
for anodic porous alumina
Croconic acid
pKa1 = 0.8, pKa2 = 2.2
?
Rhodizonic acid
pKa1 = 4.3, pKa2 = 4.7
?
Heptagonic acid
pKa1 and pKa2 = unknown
Not commercially available

Figure 1

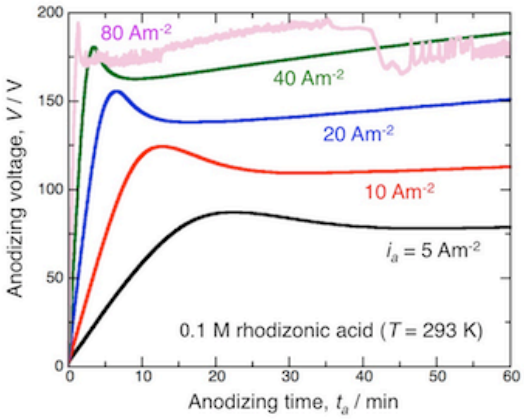
80 Am-2
40 Am-2
20 Am-2
10 Am-2
ia = 5 Am-2
0.1 M rhodizonic acid (T = 293 K)
Anodizing voltage, V / V
Anodizing time, ta / min
0
50
100
150
200
0
10
20
30
40
50
60

Figure 2

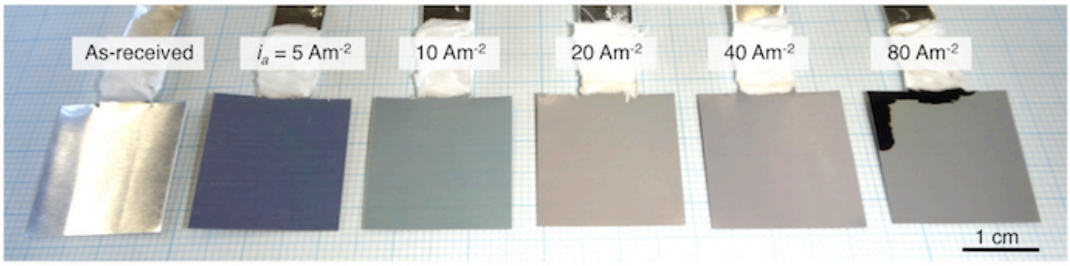

Figure 3

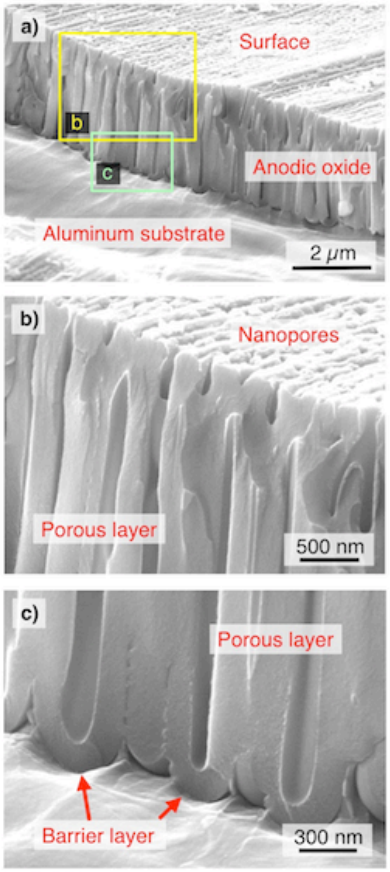
a)
Surface
b
c
Anodic oxide
Aluminum substrate
2 μm
b)
Nanopores
Porous layer
500 nm
c)
Porous layer
Barrier layer
300 nm

Figure 4

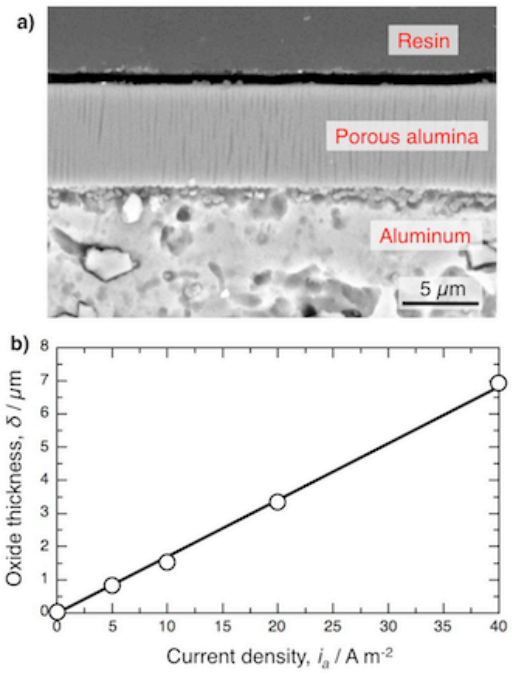
a)
Resin
Porous alumina
Aluminum
5 μm
b)
Oxide thickness, δ / μm
Current density, i_a / A m^{-2}
0
1
2
3
4
5
6
7
8
0
5
10
15
20
25
30
35
40

Figure 5

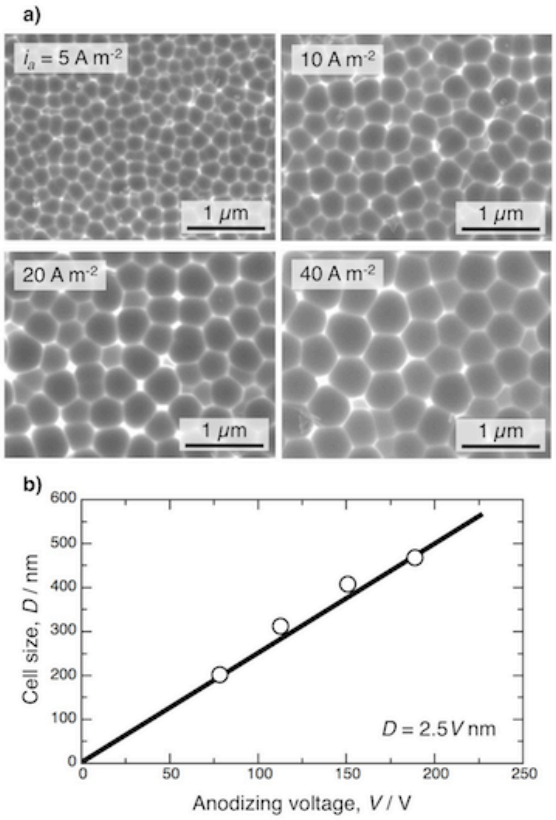
a)
i_a = 5 A m^{-2}
10 A m^{-2}
20 A m^{-2}
40 A m^{-2}
1 μm
b)
Cell size, D / nm
Anodizing voltage, V / V
D = 2.5V nm
0
100
200
300
400
500
600
50
150
250

Figure 6

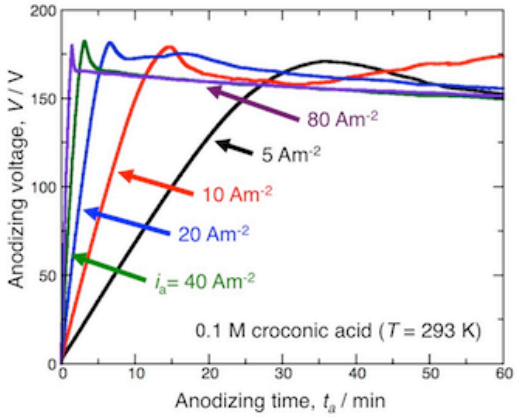
Anodizing voltage, V / V
Anodizing time, t_a / min
80 Am^{-2}
5 Am^{-2}
10 Am^{-2}
20 Am^{-2}
i_a= 40 Am^{-2}
0.1 M croconic acid (T = 293 K)
0
50
100
150
200
0
10
20
30
40
50
60

Figure 7

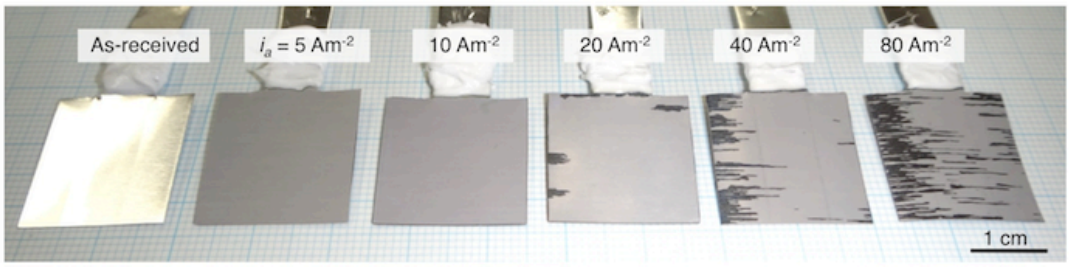

Figure 8

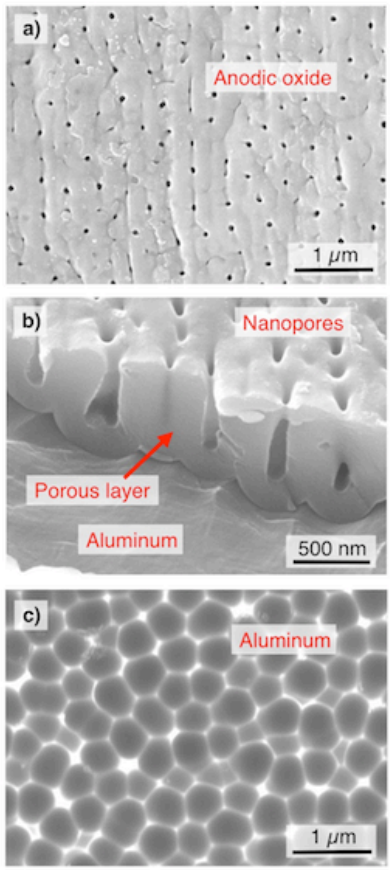
a)
Anodic oxide
1 μm
b)
Nanopores
Porous layer
Aluminum
500 nm
c)
Aluminum
1 μm

Figure 9

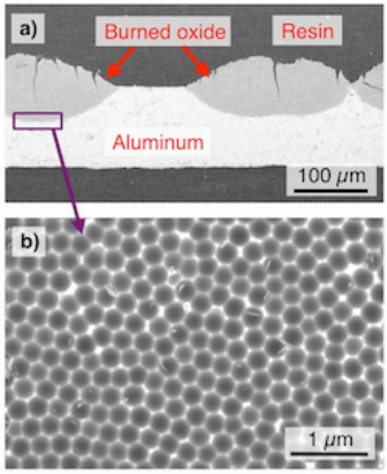

Figure 10

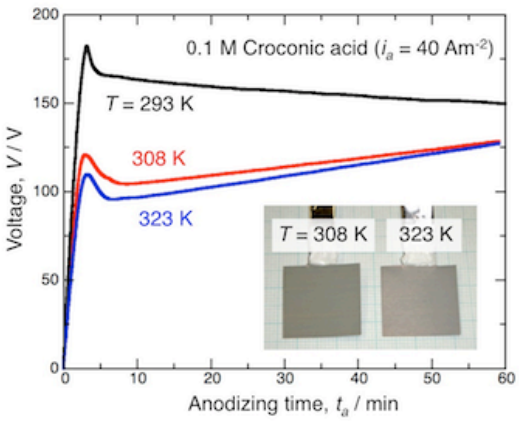
0.1 M Croconic acid (i_a = 40 Am^{-2})
T = 293 K
308 K
323 K
T = 308 K
323 K
Voltage, V / V
Anodizing time, t_a / min
0
50
100
150
200
0
10
20
30
40
50
60

Figure 11

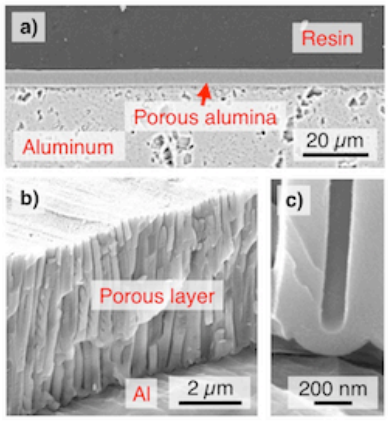
a)
Resin
Porous alumina
Aluminum
20 μm
b)
Porous layer
Al
2 μm
c)
200 nm

Figure 12